

# Seismic indices – a deep look inside evolved stars

B. Mosser<sup>1,\*</sup>

LESIA, Observatoire de Paris, PSL Research University, CNRS, Université Pierre et Marie Curie, Université Paris Diderot, 92195 Meudon, France

Received XXXX, accepted XXXX

Published online XXXX

**Key words** Stars: oscillations - Stars: interiors - Stars: evolution

Independent of stellar modelling, global seismic parameters of red giants provide unique information on the individual stellar properties as well as on stellar evolution. They allow us to measure key stellar parameters, such as the stellar mass and radius, or to derive the distance of field stars. Furthermore, oscillations with a mixed character directly probe the physical conditions in the stellar core. Here, we explain how very precise seismic indices are obtained, and how they can be used for monitoring stellar evolution and performing Galactic archeology.

Copyright line will be provided by the publisher

## 1 Introduction

Red giant seismology is one of the exquisite surprise provided by the space missions *CoRoT* and *Kepler*. From the analysis of long, continuous, ultra-precise photometric light curves, seismic indices can be derived from calibrated global seismic parameters that describe the oscillation pattern. They measure the properties of both the stellar envelope and the core. In this review, we focus on ensemble asteroseismology results that provide a wealth of global information. The analysis and modelling of individual stars have started for a handful of targets (e.g., Baudin et al. 2012; di Mauro et al. 2011; Di Mauro et al. 2015; Jiang et al. 2011; Lillo-Box et al. 2014) but are not presented here, despite the fact they are crucial for the deep understanding of the stellar interior structure and of the physical input to be considered, such as the measurement of the location of the helium second-ionization region (Miglio et al. 2010), or the measurement of differential rotation (Beck et al. 2012; Deheuvels et al. 2012). The global properties of the low-degree oscillation spectra used to derive relevant estimates of the stellar masses and radii are presented in Section 2. In Section 3, I show the rich information provided by the identification of mixed modes. They result from the coupling of gravity waves propagating in the radiative core region, with pressure waves mainly propagating in the stellar envelope, and directly reveal information from the stellar core (Bedding et al. 2011). A few results permitted by ensemble asteroseismic measurements are presented in Section 4.

## 2 Solar-like oscillations

Two seismic indices, the frequency  $\nu_{\max}$  of maximum oscillation signal and the frequency separation  $\Delta\nu$  between radial modes, can be easily defined from the structure of the low-degree oscillation pressure pattern. In this Section, we intend to show how they can be precisely determined.

### 2.1 Gravity and convection

The empirical definition of  $\nu_{\max}$  is clear. However, measuring it is more difficult, partly because  $\nu_{\max}$  depends on the observable (intensity or velocity measurements provide two different values of  $\nu_{\max}$  since the translation of relative photometric amplitude to Doppler velocity depends on frequency). In fact, we lack a precise and non-empirical definition of  $\nu_{\max}$ . In practice, the maximum of oscillation signal comes from the minimum of the product  $\eta I$ , where  $\eta$  is the damping rate and  $I$  the inertia of the modes. (e.g., Balmforth 1992; Belkacem et al. 2012). This occurs when oscillation periods are equivalent to the thermal and convective time scales.

Observations show that  $\nu_{\max}$  provides a highly-precise measurement of the stellar gravity (e.g., Morel & Miglio 2012; Morel et al. 2014; Pinsonneault et al. 2014) since it scales as the acoustic cutoff frequency (Belkacem et al. 2011; Brown et al. 1991), hence as the ratio  $g/\sqrt{T_{\text{eff}}}$ . This is verified for most of stars, except in some cases, as Procyon, where the oscillation excess power shows two humps (Arentoft et al. 2008). In the general case, from  $\nu_{\max}$  we get a reliable and precise proxy of  $M R^{-2} T_{\text{eff}}^{-1/2}$ .

\* Corresponding author: benoit.mosser@obspm.fr

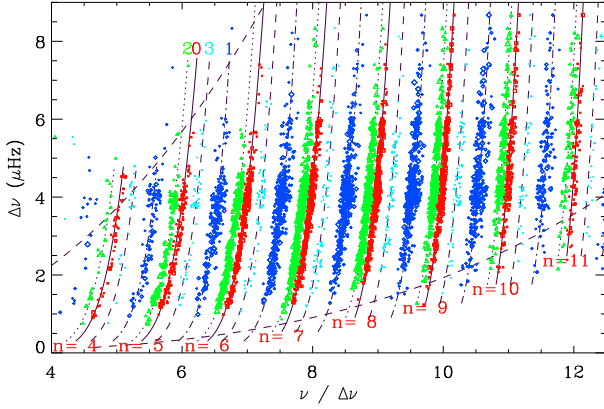


**Fig. 1** Identification of the low-degree oscillation modes of CoRoT red giants. Each color corresponds to a different mode degree (radial modes in red, dipole modes in dark blue,  $\ell = 2$  modes in green,  $\ell = 3$  modes in light blue). The solid grey lines indicate the fits of  $\varepsilon$  for each radial order  $n$ . The fits of  $d_{01}$ ,  $d_{02}$  and  $d_{03}$  are superimposed on the respective ridges (respectively dash-dot, dot, and dash lines for  $\ell = 1, 2$ , and  $3$ ). The dark dashed lines delineate the region where the modes have noticeable amplitudes. Figure from Mosser et al. (2011).

## 2.2 Homology and universal pattern

The low-degree oscillation spectrum of red giant pressure modes follows, as for other stars, the asymptotic expansion (Tassoul 1980):

$$\nu_{n,\ell} = \left( n'_\ell + \frac{A_\ell}{n'_\ell} \right) \Delta\nu_{\text{as}}, \quad \text{with } n'_\ell = n + \frac{\ell}{2} + \varepsilon_{\text{as}}, \quad (1)$$

where  $n$  is the radial order and  $\ell$  is the angular degree. The asymptotic large separation  $\Delta\nu_{\text{as}} = (2 \int_0^R dr/c)^{-1}$  measures the stellar acoustic radius. The asymptotic value of  $\varepsilon_{\text{as}}$  is  $1/4$ . The second-order coefficients  $A_\ell$  have a more complicated form.

CoRoT observations have evidenced a unique property of the red giant oscillation pattern: following the interior structure homology, the pattern can also be defined as homologous. The concept of universal red giant oscillation pattern was introduced by Mosser et al. (2011), as an alternative form to the usual asymptotic expansion (Tassoul 1980), with the observed large separation as the only free parameter. The second-order asymptotic expansion expresses as

$$\nu_{n,\ell} = \left( n + \frac{\ell}{2} + \varepsilon_{\text{obs}} + \alpha \ell + \frac{\alpha}{2} (n - n_{\text{max}})^2 \right) \Delta\nu_{\text{obs}}, \quad (2)$$

where all the parameters depend either on  $\Delta\nu_{\text{obs}}$  or on the dimensionless parameter  $n_{\text{max}} = \nu_{\text{max}}/\Delta\nu_{\text{obs}} - \varepsilon_{\text{obs}}$  (Mosser et al. 2013c): the radial offset  $\varepsilon_{\text{obs}}$  helps to locate the radial ridge; the non-radial offsets  $\alpha\ell$  express the shifts of the different degrees  $\ell$  compared to the radial modes (e.g., Corsaro et al. 2012); the term  $\alpha$  accounts for the second-order asymptotic expansion.

The signature of homology of red giants is illustrated in Fig. 1, where CoRoT red giant oscillation spectra sorted by increasing large separation values are plotted on the same graph, with a dimensionless frequency in abscissa. The alignment of the ridges, each one corresponding to a given radial order  $n$  and angular degree  $\ell$ , demonstrates the validity of Eq. (2). Contrarily, oscillation patterns in main-sequence stars could not be superposed.

Equation (2) accounts for the measurement of  $\Delta\nu_{\text{obs}}$  around  $\nu_{\text{max}}$ . The asymptotic large separation  $\Delta\nu_{\text{as}}$  corresponds to the frequency spacing at very high frequency, hence it cannot be measured. Its theoretical value is slightly larger than the observed value; the relationship between the observed and asymptotic parameters is studied in Mosser et al. (2013c). The high accuracy level reached by Eq. (2) has been shown in previous comparison work (e.g., Hekker et al. 2012; Verner et al. 2011b); the accuracy of the measurement of  $\Delta\nu_{\text{obs}}$  is better than  $0.04 \mu\text{Hz}$  for all evolutionary stages (Mosser et al. 2013a).

The measurement of  $\Delta\nu_{\text{obs}}$  is however perturbed by a modulation due to the rapid local variation of the sound speed in the stellar interior, related to the density contrast at the core boundary or to the local depression of the sound speed that occurs in the helium second-ionization region (Miglio et al. 2010). The main signature of the glitch induces a modulation of the spectrum. Ensemble analysis of this glitch has shown how it can be modelled, depending on stellar evolution (Vrard et al. 2015a). This means that we can derive glitch-free measurement of the large separation. As a result, with the large separation measured in a broad frequency range, accounting for the second-order correction of the asymptotic correction, and corrected for glitch perturbation, the measurement of the large separation provides a reliable proxy of the square root of the mean density  $\sqrt{M/R^3}$ .

## 2.3 Scaling relations

Seismic relations with  $\Delta\nu_{\text{obs}}$  and  $\nu_{\text{max}}$  can be used to provide proxies of the stellar masses and radii. The scaling relations write

$$\frac{R}{R_\odot} = \left( \frac{\nu_{\text{max}}}{\nu_{\text{ref}}} \right) \left( \frac{\Delta\nu_{\text{as}}}{\Delta\nu_{\text{ref}}} \right)^{-2} \left( \frac{T_{\text{eff}}}{T_\odot} \right)^{1/2}, \quad (3)$$

$$\frac{M}{M_\odot} = \left( \frac{\nu_{\text{max}}}{\nu_{\text{ref}}} \right)^3 \left( \frac{\Delta\nu_{\text{as}}}{\Delta\nu_{\text{ref}}} \right)^{-4} \left( \frac{T_{\text{eff}}}{T_\odot} \right)^{3/2}, \quad (4)$$

where the calibrated references  $\nu_{\text{ref}} = 3104 \mu\text{Hz}$  and  $\Delta\nu_{\text{ref}} = 138.8 \mu\text{Hz}$  are derived from the comparison with modelling (Mosser et al. 2013c), in contrast to many works that use the solar case as a reference (e.g., Silva Aguirre et al. 2011; Stello et al. 2013; Verner et al. 2011a). Large efforts are undertaken for calibrating Eqs. (3) and (4), since solar reference values provide biases in the red giant regime (e.g., Epstein et al. 2014; Miglio et al. 2012; White et al. 2011), as made clear since CoRoT observations (Kallinger et al. 2010; Mosser et al. 2010). Following Belkacem et al. (2013), we note that, for performing

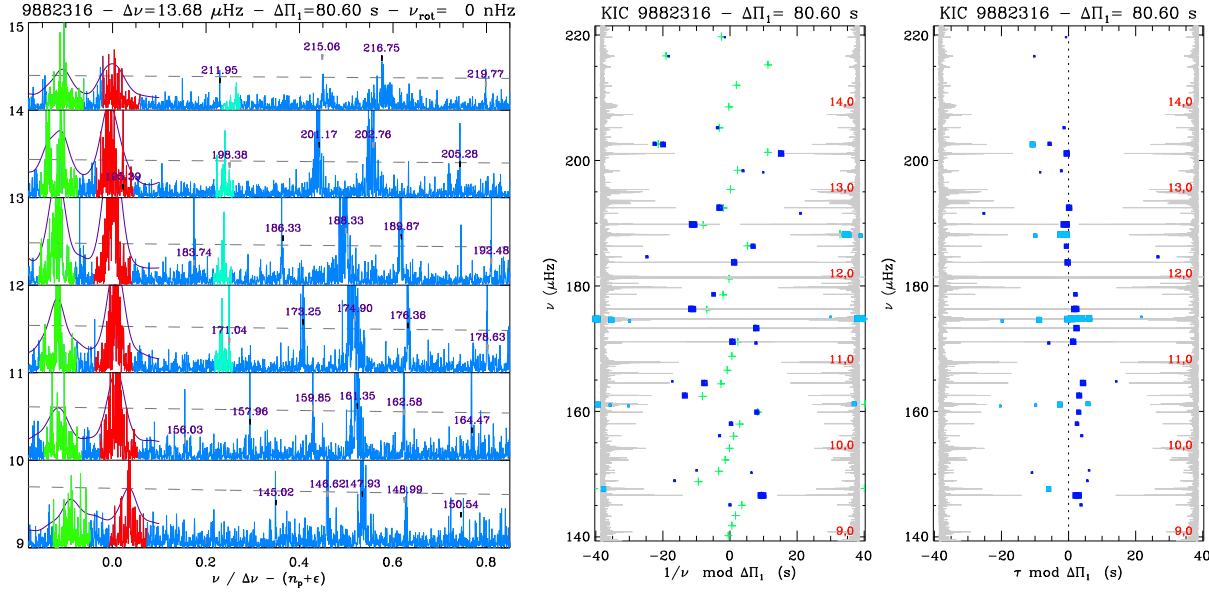


**Fig. 2** Échelle diagrams of the RGB star KIC 9882316 that shows no rotational signature. *Left*: Frequency échelle diagram as a function of  $\nu/\Delta\nu - (n + \varepsilon_p)$ . The radial order  $n$  is indicated on the y-axis. Radial modes are highlighted in red,  $\ell = 2$  modes in green, and  $\ell = 3$  modes, when observed, in light blue. Dipole mixed mode frequencies with a height larger than eight times the mean background value (grey dashed lines) are identified in  $\mu\text{Hz}$ . *Middle*: Period échelle diagram, based on  $1/\nu$  modulo  $\Delta\Pi_1$ . The most prominent mixed modes, marked with blue filled squares (in light blue for peaks in the vicinity of pure pressure modes), are automatically identified. In the background of the figure, the spectra are plotted twice and top to tail for making the mode identification easier, with  $n$  indicated for radial modes. *Right*: Stretched period échelle diagram, based on  $\tau$  modulo  $\Delta\Pi_1$ . Figure from Mosser et al. (2015)

the calibration, it is necessary to avoid confusion between the large separation  $\Delta\nu_{\text{obs}}$  measured from radial modes observed around  $\nu_{\text{max}}$ , the asymptotic large separation  $\Delta\nu_{\text{as}}$ , and the dynamical frequency  $\nu_0$  that scales with  $\sqrt{M/R^3}$ .

### 3 Dipole mixed modes

Mixed modes allow us to detect the gravity modes that probe the stellar core in a much more efficient way compared to the Sun (e.g., Belkacem et al. 2009).

#### 3.1 Asymptotic expansion

Shibahashi (1979) and Unno et al. (1989) derived an implicit asymptotic relation for mixed modes in case of weak coupling, which expresses as

$$\tan \theta_p = q \tan \theta_g. \quad (5)$$

The phases  $\theta_p$  and  $\theta_g$  refer, respectively, to the pressure- and gravity-wave contributions, and  $q$  is the coupling factor between them. Mosser et al. (2015) write them

$$\theta_p = \pi \frac{\nu - \nu_p}{\Delta\nu_n} \quad \text{and} \quad \theta_g = \pi \frac{1}{\Delta\Pi_1} \left( \frac{1}{\nu} - \frac{1}{\nu_g} \right), \quad (6)$$

where  $\nu_p$  and  $\nu_g$  are the asymptotic frequencies of pure pressure and gravity modes, respectively,  $\Delta\nu_n$  is the frequency difference between two consecutive pure pressure radial modes (the subscript  $n$  means that small variations of

the large separation with the radial order can be accounted for), and  $\Delta\Pi_1$  is the asymptotic period spacing of gravity modes. Equation (6) can be used at any order of the asymptotic expansions for the pure pressure and gravity contributions. For instance, these expressions may include the signature of acoustic or buoyancy glitches (Mosser et al. 2015).

#### 3.2 Period spacing and rotational splitting

The derivation of the implicit asymptotic expansion provides an analytical form of the period spacing between two consecutive mixed modes, which writes  $\Delta P/\Delta\Pi_1 = \zeta$ , with

$$\zeta = \left[ 1 + \frac{1}{q} \frac{\nu^2 \Delta\Pi_1}{\Delta\nu_n} \frac{\cos^2 \pi \frac{1}{\Delta\Pi_1} \left( \frac{1}{\nu} - \frac{1}{\nu_g} \right)}{\cos^2 \pi \frac{\nu - \nu_p}{\Delta\nu_n}} \right]^{-1}. \quad (7)$$

Interestingly, this expression matches the first-order asymptotic expansion derived by Deheuvels et al. (2015) for expressing the mixed-mode rotational splitting. Following Goupil et al. (2013) and Deheuvels et al. (2015), the rotational splitting of mixed modes expresses

$$\delta\nu_{\text{rot}} = \delta\nu_{\text{rot,g}} \zeta + \delta\nu_{\text{rot,p}} (1 - \zeta), \quad (8)$$

where  $\delta\nu_{\text{rot,g}}$  and  $\delta\nu_{\text{rot,p}}$  are the rotational splittings related to pure gravity or pure pressure modes. The measurement of rotational splittings and the derivation of the mean core rotation are discussed in Mosser et al. (2012b). Specific cases are discussed in Beck et al. (2012), Deheuvels et al. (2012), and Deheuvels et al. (2014).

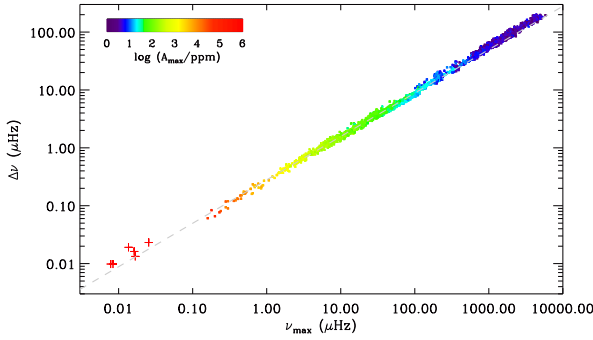


**Fig. 3**  $\nu_{\max} - \Delta\nu_{\text{obs}}$  relation, with CoRoT and *Kepler* data. Plusses are red supergiants showing observed by Kiss et al. (2006), with  $\Delta\nu_{\text{obs}}$  and  $\nu_{\max}$  derived from a combination of the frequencies. The colors code the mean maximum amplitude  $A_{\max}$  of the radial oscillations. The grey dashed line has a slope 3/4.

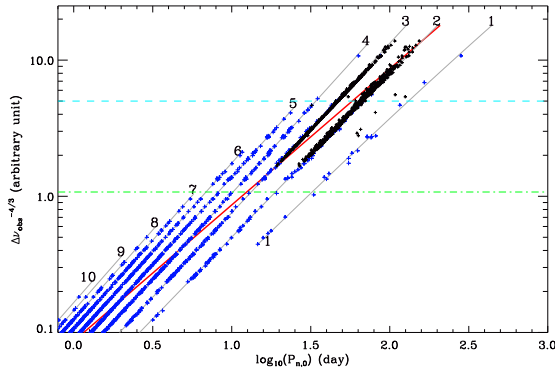


**Fig. 4** Period-luminosity relations of radial modes of AGB and RGB stars observed with *Kepler* (blue pluses) and OGLE (black symbols). The proxy of the luminosity is derived from  $\Delta\nu_{\text{obs}}^{-4/3}$ . Each sequence, corresponding to a fixed radial order, is fitted with the model provided by Eq. (2) extrapolated to low frequency (gray solid lines). The thick red line indicates the location of  $\nu_{\max}$ . The blue dashed line corresponds to the tip of the RGB. Figure from Mosser et al. (2013b).

### 3.3 Asymptotic period spacing

The previous developments provide the theoretical basis for the thorough understanding of the mixed modes. Following Mosser et al. (2015), the function  $\zeta$  is used to turn the frequencies into periods  $\tau$ , with  $d\tau = -d \log(1/\nu)/\zeta$ . From the integration of this change of variable we derive corrected periods  $\tau$  of mixed modes, called stretched periods. Échelle diagrams based on  $\tau$  show the structure of the gravity modes contributing to the mixed modes (Fig. 2). This allows the most accurate measurement of the asymptotic period spacing even when rotation splittings are important (Vrard et al. 2015b) and emphasizes the signature of the buoyancy glitches, namely rapid variation of the Brunt-Väisälä frequency in the radiative core.

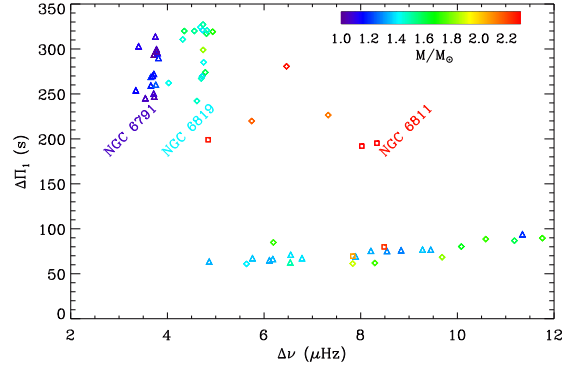


**Fig. 5**  $\Delta\Pi_1 - \Delta\nu$  relations for red giants in three open clusters observed by *Kepler* (NGC 6791,  $\triangle$ ; 6819,  $\diamond$ , with three blue stragglers; 6811,  $\square$ ). Tracks on the RGB are superimposed, but not in the red clump. Figure from Vrard et al. (2015b).

## 4 Seismic indices

Global seismic parameters can be used as seismic indices for characterizing stars and performing ensemble asteroseismology.

### 4.1 Stellar evolution up to the AGB

From the scaling relations Eqs. (3) and (4), we derive

$$\Delta\nu_{\text{obs}} \simeq \Delta\nu_{\text{as}} \propto M^{-1/4} T_{\text{eff}}^{3/8} \nu_{\max}^{3/4}. \quad (9)$$

On the red and asymptotic giant branches, all low-mass stars are present at all evolutionary stages, so that the mass play no role in this relation. Consequently,  $\Delta\nu_{\text{obs}}$  scales as  $\nu_{\max}^{3/4}$  (Fig. 3). The validity of Eq. (9) over more than six decades in frequency indicates that the stellar red giant populations observed by CoRoT or *Kepler* constitute a set of stars homogeneous enough to mimic stellar evolution.

This result extrapolated to very low  $\nu_{\max}$ , with Eq. (2) iteratively adapted to fit the low-frequency oscillation spectra, was used for demonstrating that period-luminosity relations in semi-regular variables are drawn by low-degree low-radial-order solar-like oscillations (Mosser et al. 2013b). When the large separation decreases, the radial orders of the observed modes decrease too, down to  $n_{\max} = 2$  (Fig. 4). Interpreting oscillations in semi-regular variables as solar-like oscillations can be used to investigate with a firm physical basis the time series obtained from ground-based microlensing surveys. This will provide improved distance measurements, since an accurate measurement of the stellar radius permits an accurate use of the Stefan-Boltzmann law, and opens the way to extragalactic asteroseismology, with the observations of M giants in the Magellanic Clouds. Mosser et al. (2013b) have also shown that the acceleration of the external layers of red giant with solar-like oscillations is about the same order of magnitude as the surface gravity when the stars reach the tip of the RGB: global oscillations play a role in the mass-loss process.



## 4.2 $\Delta\nu - \Delta\Pi_1$ diagram

The measurement of  $\Delta\Pi_1$  provides a unique view on the physical properties in the stellar core (Mosser et al. 2012a) and reveals clear differences between evolutionary stages (Mosser et al. 2014). The analysis, now expanded to large populations by Vrad et al. (2015b) with about 5 000 red giants, shows the influence of the stellar mass and metallicity on the evolution on the RGB in the  $\Delta\nu - \Delta\Pi_1$  diagram. In Fig. 5, we illustrate the mass dependence of the  $\Delta\nu - \Delta\Pi_1$  relation for core-helium burning stars in three open clusters (Miglio et al. 2012; Stello et al. 2010). Evolution tracks largely depend on the mass, with massive stars in NGC 6811 in the secondary clump. Three stars of NGC 6819, much more massive than expected, are confirmed as blue stragglers (Corsaro et al. 2012). The highly precise evolutionary tracks in the  $\Delta\nu - \Delta\Pi_1$  diagram can now be used to constrain stellar evolution modelling (e.g., Bossini et al. 2015; Lagarde et al. 2015).

## 4.3 Rotation

Rotation also benefitted from ensemble asteroseismology. Mosser et al. (2012b) have shown a significant spin-down of the core rotation with evolution on the RGB. Mechanisms able to efficiently transfer angular momentum from the core to the envelope have been investigated (e.g., Eggenberger et al. 2012); the role of mixed modes for spinning down the core rotation is underlined by Belkacem et al. (2015a,b). This topic, as all others, now benefit from supplementary non-seismic measurements and from theoretical developments, to make the best of seismic indices.

*Acknowledgements.* We acknowledge the CoRoT and *Kepler* teams, whose efforts made these results possible. We acknowledge financial support from the Programme National de Physique Stellaire (CNRS/INSU) and from the ANR program IDEE.

## References

- Arentoft, T., Kjeldsen, H., Bedding, T. R., et al. 2008, *ApJ*, 687, 1180
- Balmforth, N. J. 1992, *MNRAS*, 255, 603
- Baudin, F., Barban, C., Goupil, M. J., et al. 2012, *A&A*, 538, A73
- Beck, P. G., Montalbán, J., Kallinger, T., et al. 2012, *Nature*, 481, 55
- Bedding, T. R., Mosser, B., Huber, D., et al. 2011, *Nature*, 471, 608
- Belkacem, K., Dupret, M. A., Baudin, F., et al. 2012, *A&A*, 540, L7
- Belkacem, K., Goupil, M. J., Dupret, M. A., et al. 2011, *A&A*, 530, A142
- Belkacem, K., Marques, J. P., Goupil, M. J., et al. 2015a, *A&A*, 579, A31
- Belkacem, K., Marques, J. P., Goupil, M. J., et al. 2015b, *A&A*, 579, A30
- Belkacem, K., Samadi, R., Goupil, M. J., et al. 2009, *A&A*, 494, 191
- Belkacem, K., Samadi, R., Mosser, B., Goupil, M.-J., & Ludwig, H.-G. 2013, in *Astronomical Society of the Pacific Conference Series*, Vol. 479, *Progress in Physics of the Sun and Stars: A New Era in Helio- and Asteroseismology*, ed. H. Shibahashi & A. E. Lynas-Gray, 61
- Bossini, D., Miglio, A., Salaris, M., et al. 2015, *MNRAS*, 453, 2290
- Brown, T. M., Gilliland, R. L., Noyes, R. W., & Ramsey, L. W. 1991, *ApJ*, 368, 599
- Corsaro, E., Stello, D., Huber, D., et al. 2012, *ApJ*, 757, 190
- Deheuvels, S., Ballot, J., Beck, P. G., et al. 2015, *A&A*, 580, A96
- Deheuvels, S., Doğan, G., Goupil, M. J., et al. 2014, *A&A*, 564, A27
- Deheuvels, S., García, R. A., Chaplin, W. J., et al. 2012, *ApJ*, 756, 19
- di Mauro, M. P., Cardini, D., Catanzaro, G., et al. 2011, *MNRAS*, 415, 3783
- Di Mauro, M. P., Ventura, R., Cardini, D., et al. 2015, *ArXiv e-prints*
- Eggenberger, P., Montalbán, J., & Miglio, A. 2012, *A&A*, 544, L4
- Epstein, C. R., Elsworth, Y. P., Johnson, J. A., et al. 2014, *ApJ*, 785, L28
- Goupil, M. J., Mosser, B., Marques, J. P., et al. 2013, *A&A*, 549, A75
- Hekker, S., Elsworth, Y., Mosser, B., et al. 2012, *A&A*, 544, A90
- Jiang, C., Jiang, B. W., Christensen-Dalsgaard, J., et al. 2011, *ApJ*, 742, 120
- Kallinger, T., Weiss, W. W., Barban, C., et al. 2010, *A&A*, 509, A77
- Kiss, L. L., Szabó, G. M., & Bedding, T. R. 2006, *MNRAS*, 372, 1721
- Lagarde, N., Bossini, D., Miglio, A., Vrad, M., & Mosser, B. 2015, *ArXiv e-prints*
- Lillo-Box, J., Barrado, D., Moya, A., et al. 2014, *A&A*, 562, A109
- Miglio, A., Brogaard, K., Stello, D., et al. 2012, *MNRAS*, 419, 2077
- Miglio, A., Montalbán, J., Carrier, F., et al. 2010, *A&A*, 520, L6
- Morel, T. & Miglio, A. 2012, *MNRAS*, 419, L34
- Morel, T., Miglio, A., Lagarde, N., et al. 2014, *A&A*, 564, A119
- Mosser, B., Belkacem, K., Goupil, M., et al. 2011, *A&A*, 525, L9
- Mosser, B., Belkacem, K., Goupil, M., et al. 2010, *A&A*, 517, A22
- Mosser, B., Belkacem, K., & Vrad, M. 2013a, in *EAS Publications Series*, Vol. 63, *EAS Publications Series*, ed. G. Alecian, Y. Lebreton, O. Richard, & G. Vauclair, 137–150
- Mosser, B., Benomar, O., Belkacem, K., et al. 2014, *A&A*, 572, L5
- Mosser, B., Dziembowski, W. A., Belkacem, K., et al. 2013b, *A&A*, 559, A137
- Mosser, B., Goupil, M. J., Belkacem, K., et al. 2012a, *A&A*, 540, A143
- Mosser, B., Goupil, M. J., Belkacem, K., et al. 2012b, *A&A*, 548, A10
- Mosser, B., Michel, E., Belkacem, K., et al. 2013c, *A&A*, 550, A126
- Mosser, B., Vrad, M., Belkacem, K., Deheuvels, S., & Goupil, M. J. 2015, *A&A*, 584, A50
- Pinsonneault, M. H., Elsworth, Y., Epstein, C., et al. 2014, *ApJS*, 215, 19
- Shibahashi, H. 1979, *PASJ*, 31, 87
- Silva Aguirre, V., Chaplin, W. J., Ballot, J., et al. 2011, *ApJ*, 740, L2

- Stello, D., Basu, S., Bruntt, H., et al. 2010, *ApJ*, 713, L182
- Stello, D., Huber, D., Bedding, T. R., et al. 2013, *ApJ*, 765, L41
- Tassoul, M. 1980, *ApJS*, 43, 469
- Unno, W., Osaki, Y., Ando, H., Saio, H., & Shibahashi, H. 1989, *Nonradial oscillations of stars*, ed. Unno, W., Osaki, Y., Ando, H., Saio, H., & Shibahashi, H.
- Verner, G. A., Chaplin, W. J., Basu, S., et al. 2011a, *ApJ*, 738, L28
- Verner, G. A., Elsworth, Y., Chaplin, W. J., et al. 2011b, *MNRAS*, 415, 3539
- Vrard, M., Mosser, B., Barban, C., et al. 2015a, *A&A*, 579, A84
- Vrard, M., Mosser, B., & Samadi, R. 2015b, *ArXiv e-prints*
- White, T. R., Bedding, T. R., Stello, D., et al. 2011, *ApJ*, 743, 161